Supporting Information

Defective $Mn_xZr_{1-x}O_2$ solid solution for the catalytic oxidation of toluene: Insights into the oxygen vacancy contribution

Xueqin Yang,[†,‡] Xiaolin Yu,[*,†,‡] Meizan Jing,[§] Weiyu Song,[§] Jian Liu,[§] Maofa Ge,[*,†,#]

[‡]

[†]State Key Laboratory for Structural Chemistry of Unstable and Stable Species, Beijing National Laboratory for Molecular Sciences (BNLMS), CAS Research/Education Center for Excellence in Molecular Sciences, Institute of Chemistry, Chinese Academy of Sciences, Beijing 100190, P. R. China

[‡]University of Chinese Academy of Sciences, Beijing 100049, P. R. China

[§]State Key Laboratory of Heavy Oil Processing, College of Science, China University of Petroleum-Beijing, Beijing 102249, P. R. China

[#]Center for Excellence in Regional Atmospheric Environment, Institute of Urban Environment, Chinese Academy of Sciences, Xiamen, 361021, P. R. China

*Email: icecoolyu@iccas.ac.cn; gemaofa@iccas.ac.cn

1. Catalyst characterization

The powder X-ray diffraction (XRD) patterns were collected using a D/max 2500 X-ray powder diffractometer at a scan rate (2θ) of 2° min^{-1} with Cu Kα radiation operated at 40 kV and 200 mA. The Brunauer-Emmett-Teller (BET) surface area, pore volume and pore size distribution of samples were measured by an autosorb-iQ instrument. Prior to the measurement, the samples were degassed at 473 K for 2.5 h. Inductively coupled plasma mass spectrometry (Thermo iCAP RQ) was carried out to determine the actual values of the Mn/Zr amounts in samples. The high-resolution transmission electron microscopy (HRTEM) was conducted using a JEM-2011F operated at 200 kV. X-ray photoelectron spectroscopy (XPS) analysis was performed on an ESCALAB250XI with Al Kα radiation. X-ray absorption spectroscopy (XAS) was performed at the 4B9A beamline, Beijing Synchrotron Radiation Facility (BSRF). H_2-TPR and O_2-TPD tests were carried out on an AutoChem HP 2950 and II 2920, respectively. For H_2-TPR, 100 mg samples were pretreated in an Ar flow at 200°C for 30 min. Then, the samples were reduced in a flow of 10% H_2/Ar (50 cm^3 min^{-1}) and the temperature was increased from 50 to 700 °C at a heating rate of 10 °C min^{-1}. Prior to O_2-TPD, 100 mg samples was treated in an Ar flow at 300 °C for 30 min and then oxygen adsorption proceeded with exposure to 5 % O_2/He (50 cm^3 min^{-1}) for 30 min. After that, the samples were purged in a He flow (30 cm^3 min^{-1}) and kept for 60 min. Then, the temperature was increased from 50 to 800 °C at a heating rate of 10 °C min^{-1}. The in situ diffuse reflectance FTIR spectroscopy (DRIFTS) was recorded in Nicolet iS50 in the range of 1000 - 4000 cm^{-1} with 32 scans at a resolution of 4 cm^{-1}. Prior to each measurement, all samples were pretreated at 240 ºC for 2 h in a N_2 flow to remove any surface impurities. The background spectrum was subtracted from each spectrum, respectively. The samples were tested at 240 ºC under the following conditions: 1000 ppm toluene and 20% O_2 balanced by N_2. The total flow rate was 50 mL min^{-1}.

2. Computational detail

All calculations were based on the density functional theory (DFT) and performed with the Vienna *ab initio* simulation package (VASP) code.[1] The exchange and correlation energy functional was expressed in the GGA-PBE.[2] Projector-augmented wave method was used to describe the interactions between ions and electrons.[3-4] The valence electrons were solved in the plane-wave on basis with a cutoff energy of 400 eV.[5] The convergence criteria for the energy calculation and structure optimization were set to 1.0×10^{-5} eV and a force tolerance of 0.01 eV/Å, respectively. The Monkhorst-Pack k-point mesh for the Brillouin zone sampling was performed using a $3 \times 3 \times 1$ mesh with Gaussian smearing set to 0.05 eV.[5-7]

The most stable (-111) and (111) surfaces of monoclinic and cubic zirconia were chosen for the calculations respectively, which consisted 12 atomic layers (four O-Zr-O trilayers) (Figure 1). [8-9] The (1×1) and (2×2) unit cells were used for m-ZrO_2 (-111) and c-ZrO_2 (111), respectively.[7, 10] In order to minimize the interaction between distinct slab surfaces, the vacuum space that perpendicular to the surface was set to 15 Å. During geometry optimization, the top six atom layers of zirconia were relaxed, while bottom six atom layers were fixed in their bulk positions. The adsorption energy was defined by:

$$E_{ads} = E(\text{adsorbate/surface}) - E(\text{adsorbate}) - E(\text{surface}) \quad \text{(S1)}$$

where $E(\text{adsorbate/surface})$ E(adsorbate/surface) is the total energy of a surface interacting with adsorbate, $E(\text{adsorbate})$ and $E(\text{surface})$ are the energies of the isolated adsorbate and clean surface, respectively. Therefore, a negative value means exothermic adsorption. The more negative the adsorption energy, the stronger the adsorption.[11] The oxygen vacancy formation energy was calculated by:

$$E_{O_v} = E_{\text{surface-}O_v} + \frac{1}{2}E_{O_2} - E_{\text{surface}} \quad \text{(S2)}$$

where $E_{surface}$ is the energy of perfect surface, $E_{surface\text{-}O_v}$ is the energy of defective surface with an oxygen vacancy and E_{O_2} is the energy of a gas-phase O_2.

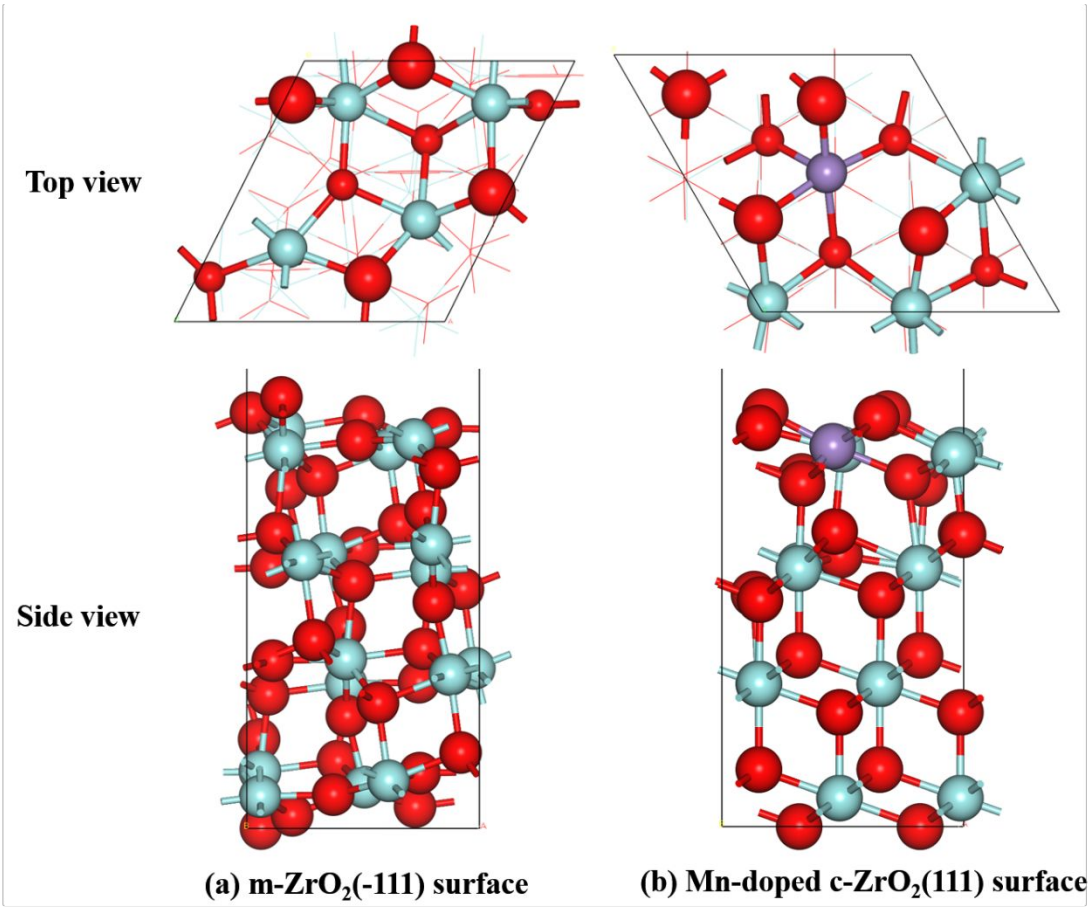

Figure S1. The optimized structures of (a) m-ZrO_2 (-111) and (b) Mn-doped c-ZrO_2 (111) surface.

3. Calculation of Weisz-Prater Criterion:

The mass-transfer effects were checked by the Weisz-Prater Criterion ($N_{w\text{-}p}$). If $N_{w\text{-}p} = \frac{r_a R_p^2}{C_s D_{eff}} < 0.3$, then internal diffusion effects can be neglected.[12-14] (S3)

Where r_a = reaction rate per volume of catalyst, mol/(m^3 s)

R_p = catalyst particle radius, m

C_s = reactant concentration at the surface of the catalyst, mol/m^3

D_{eff} = effective gas phase diffusivity, m^2/s.

The effective diffusivity D_{eff} is related to the mean free path (λ , m).

$$\lambda = \frac{k_B T}{\sqrt{2}\pi d^2 P_{toluene}} \tag{S4}$$

k_B = the Boltzmann constant, J/K

$P_{toluene}$ = partial pressure of toluene, Pa

d = diameter of toluene, m

If the mean free path (λ) is much larger than the pore sizes of the catalysts (d_p), the pore diffusion will be dominated by Knudsen diffusion.

$$D_{eff} \cong D_{Kn} = \overline{\upsilon}\frac{d_p}{3} \tag{S5}$$

$$\overline{\upsilon} = \left(\frac{8RT}{\pi M}\right)^{1/2} \tag{S6}$$

D_{Kn} = the Knudsen diffusivity, m^2/s

$\overline{\upsilon}$ = the mean velocity of the gas phase toluene, m/s

M = molar mass of toluene, kg/mol.

In the current work, a total gas flow rate of 50 mL min^{-1} and an average catalyst particle size of 0.26 mm were employed for the kinetic study. The concentration of

toluene employed in the feed gas was 1000 ppm. For ZrO_2 catalyst, the mean free path (λ) was 2.36×10^4 nm at 295 K and is much larger than the pore sizes of ZrO_2 catalyst (d_p = 6.5 nm). Therefore,

$$D_{eff} \cong D_{Kn} = \overline{\upsilon}\frac{d_p}{3} = \frac{d_p}{3}\left(\frac{8RT}{\pi M}\right)^{1/2} = 7.88\times10^{-7}\ \mathrm{m^2/s}$$

$$N_{w\text{-}p} = 0.016 << 0.3$$

For $Mn_{0.5}Zr_{0.95}O_2$ catalyst, the mean free path (λ) was 2.49×10^4 nm at 245 K and is much larger than the pore sizes of $Mn_{0.5}Zr_{0.95}O_2$ catalyst (d_p = 3.8 nm). Therefore,

$$D_{eff} \cong D_{Kn} = \overline{\upsilon}\frac{d_p}{3} = \frac{d_p}{3}\left(\frac{8RT}{\pi M}\right)^{1/2} = 4.40\times10^{-7}\ \mathrm{m^2/s}$$

$$N_{w\text{-}p} = 0.087 << 0.3$$

For $Mn_{0.1}Zr_{0.9}O_2$ catalyst, the mean free path (λ) was 2.44×10^4 nm at 235 K and is much larger than the pore sizes of $Mn_{0.5}Zr_{0.95}O_2$ catalyst (d_p = 3.8 nm). Therefore,

$$D_{eff} \cong D_{Kn} = \overline{\upsilon}\frac{d_p}{3} = \frac{d_p}{3}\left(\frac{8RT}{\pi M}\right)^{1/2} = 4.35\times10^{-7}\ \mathrm{m^2/s}$$

$$N_{w\text{-}p} = 0.065 << 0.3$$

For $Mn_{0.2}Zr_{0.8}O_2$ catalyst, the mean free path (λ) was 2.47×10^4 nm at 215 K and is much larger than the pore sizes of $Mn_{0.5}Zr_{0.95}O_2$ catalyst (d_p = 3.4 nm). Therefore,

$$D_{eff} \cong D_{Kn} = \overline{\upsilon}\frac{d_p}{3} = \frac{d_p}{3}\left(\frac{8RT}{\pi M}\right)^{1/2} = 3.81\times10^{-7}\ \mathrm{m^2/s}$$

$$N_{w\text{-}p} = 0.090 << 0.3$$

For $Mn_{0.3}Zr_{0.7}O_2$ catalyst, the mean free path (λ) was 2.45×10^4 nm at 205 K and is much larger than the pore sizes of $Mn_{0.5}Zr_{0.95}O_2$ catalyst (d_p = 3.4 nm). Therefore,

$$D_{eff} \cong D_{Kn} = \overline{\upsilon}\frac{d_p}{3} = \frac{d_p}{3}\left(\frac{8RT}{\pi M}\right)^{1/2} = 3.77\times10^{-7}\ m^2/s$$

$$N_{w\text{-}p} = 0.079 << 0.3$$

Therefore, the diffusion effect for $Mn_xZr_{1-x}O_2$ catalysts could be neglected during the kinetic experiment. There were no significant mass transfer limitations in our catalytic system.

4. Results

Table S1. Physical-chemical and toluene catalytic properties of MB-x catalysts

Samples	S_{BET} (m^2/g)	Total pore (cm^3/g)	Pore diameter (nm)	T_{50} (°C)	T_{90} (°C)	Conversion at 210 °C (%)	R_s at 210 °C [a] (mmol h^{-1} m^{-2})	D_{Rw} at 210 °C [b] (mmol g^{-1} h^{-1})	D_{Rsa} at 210 °C [c] (mmol h^{-1})
MB-0.05	106.8	0.31	7.8	283	311	0.54	1.37×10^{-4}	0.15×10^{-2}	0.79×10^{-6}
MB-0.1	106.4	0.28	6.5	276	301	1.13	2.84×10^{-4}	1.83×10^{-2}	1.82×10^{-6}
MB-0.2	93.0	0.29	7.8	260	282	2.23	6.41×10^{-4}	8.23×10^{-2}	6.32×10^{-6}
MB-0.3	87.8	0.27	7.8	252	267	3.35	10.2×10^{-4}	13.7×10^{-2}	12.4×10^{-6}

[a] Specific toluene reaction rate of MB-x samples estimated at 210 °C. [b] The differential reaction rate per unit weight at 210 °C between $Mn_xZr_{1-x}O_2$ and MB-x. [c] The differential reaction rate per unit surface area at 210 °C between $Mn_xZr_{1-x}O_2$ and MB-x.

Table S2. O_2 adsorption energy, oxygen vacancy formation energy and O-O bond length on different Zr and O sites of m-ZrO_2 (-111) surface.

Site (Zr/O)	1	2	3	4
E_{ov} (eV)	5.84	5.96	5.91	6.13
$E_{O2\text{-}ads}$ (eV)	0.37	0.35	0.33	0.36
O-O bond length (Å)	1.23	1.24	1.24	1.24

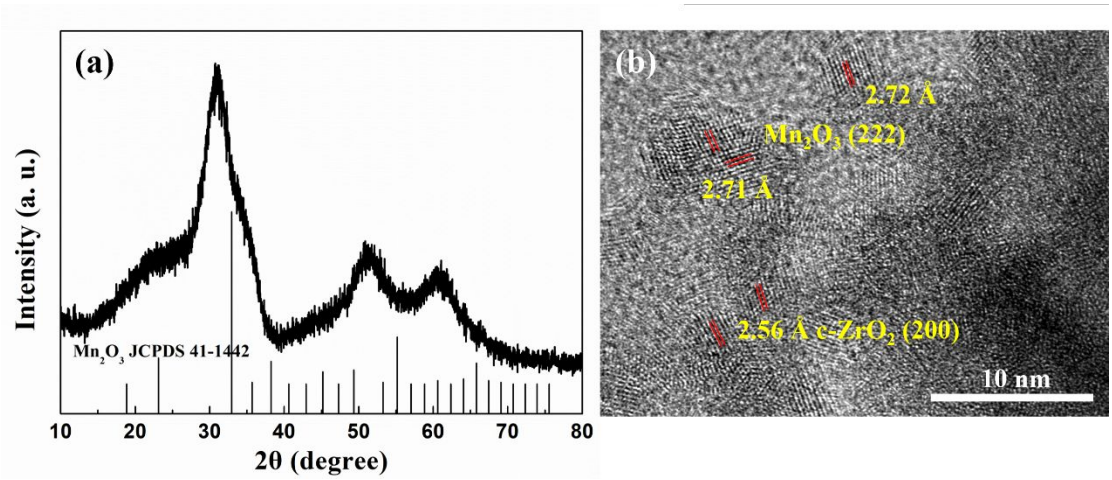

Figure S2. (a) XRD patterns and (b) HRTEM image of $Mn_{0.4}Zr_{0.6}O_2$ sample.

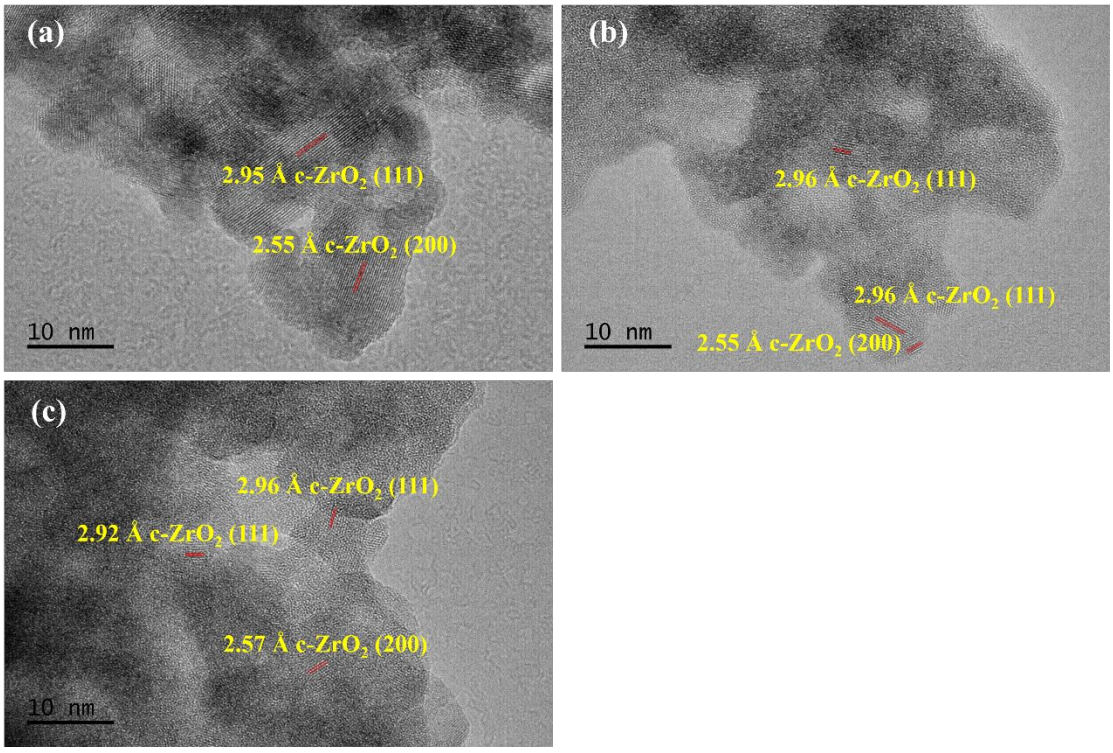

Figure S3. HRTEM image of (a) $Mn_{0.05}Zr_{0.95}O_2$, (b) $Mn_{0.1}Zr_{0.9}O_2$ and (c) $Mn_{0.2}Zr_{0.8}O_2$ samples.

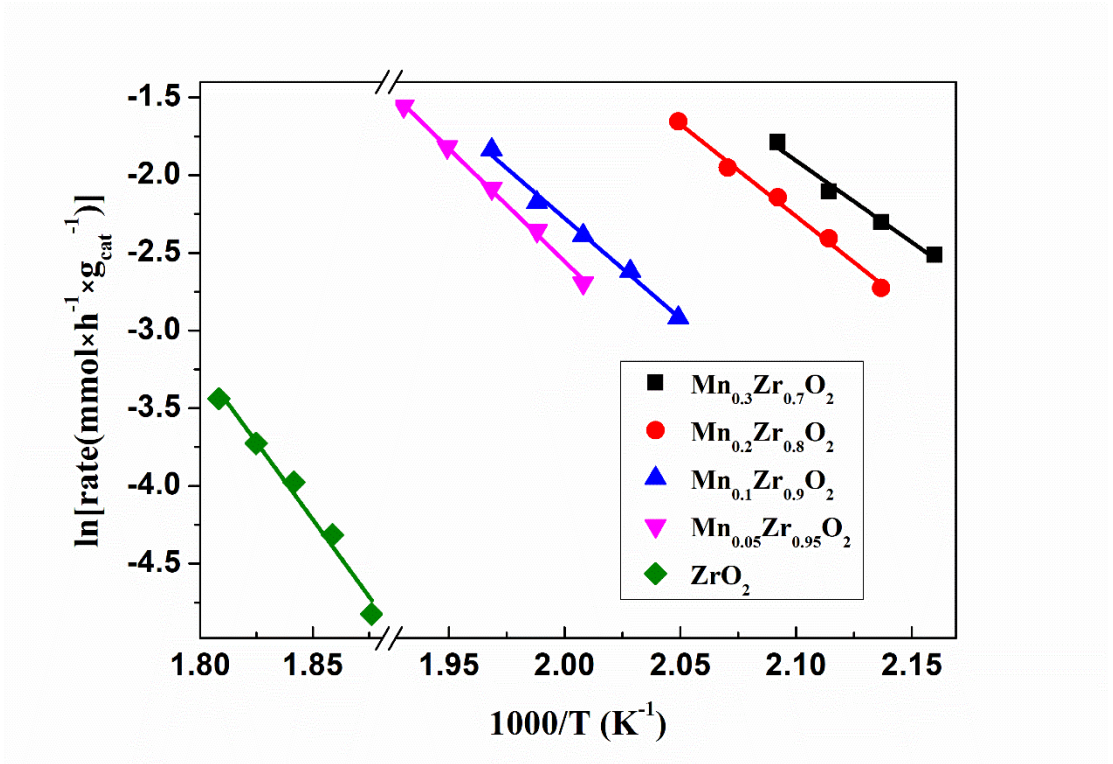

Figure S4. Arrhenius plots of toluene reaction rates over $Mn_xZr_{1-x}O_2$ catalysts.

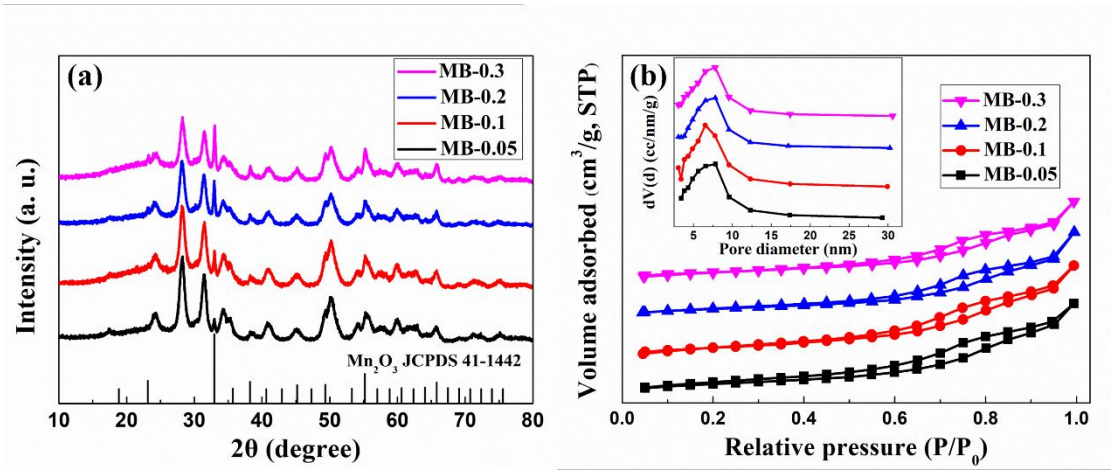

Figure S5. (a) XRD patterns and (b) Nitrogen adsorption-desorption isotherms together with corresponding pore-size distribution curves of MB-x catalysts.

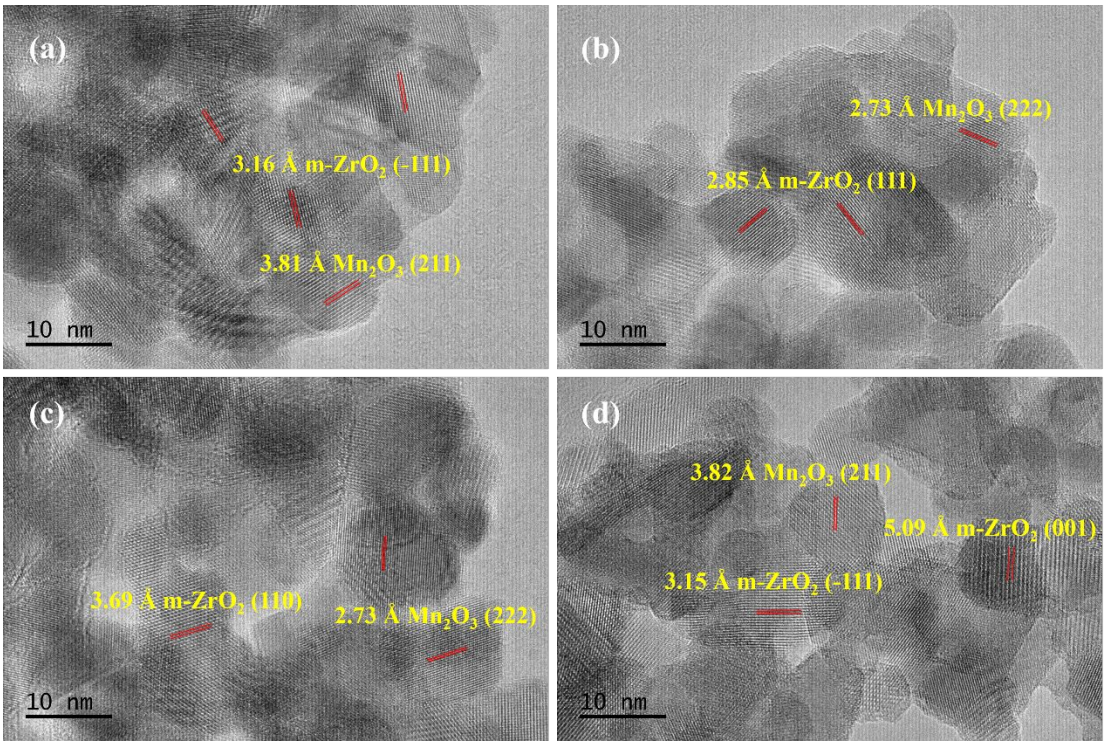

Figure S6. HRTEM image of (a) MB-0.05, (b) MB-0.1, (c) MB-0.2 and (d) MB-0.3 samples.

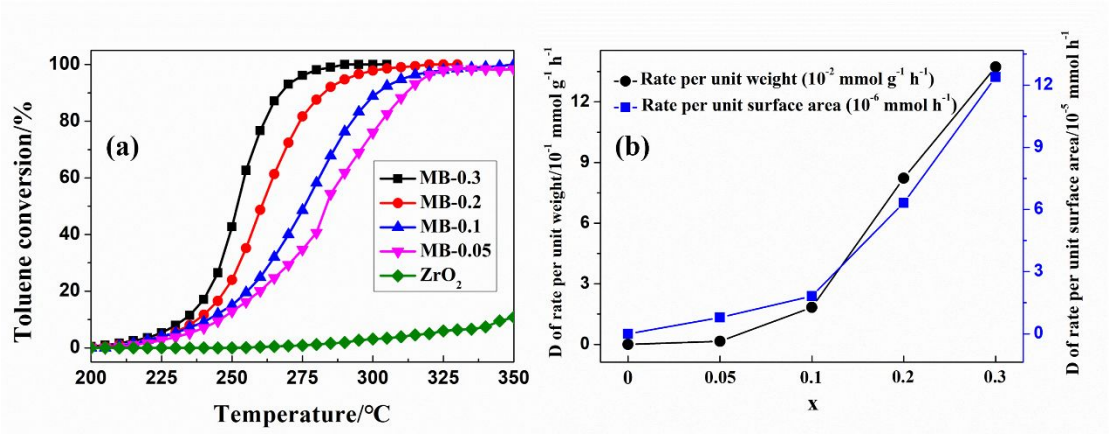

Figure S7. (a) Toluene conversion over MB-x catalysts and (b) the relationship between differential reaction rates per unit weight (D_{Rw}) and unit surface area (D_{Rsa}) of samples and manganese content x.

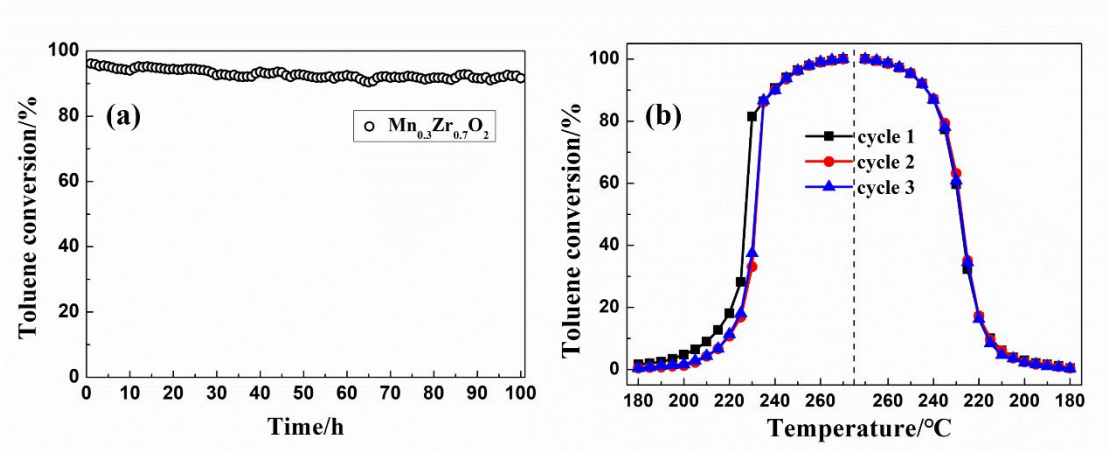

Figure S8. (a) The durability test of the $Mn_{0.3}Zr_{0.7}O_2$ catalyst at 240 ºC and (b) The catalytic stability as a function of temperature over $Mn_{0.3}Zr_{0.7}O_2$ catalyst in the temperature cycle experiment. The sample was repeated three times. Reaction conditions: 1000 ppm toluene, 20 % O_2, WHSV = 60 000 mL g_{cat}^{-1} h^{-1}.

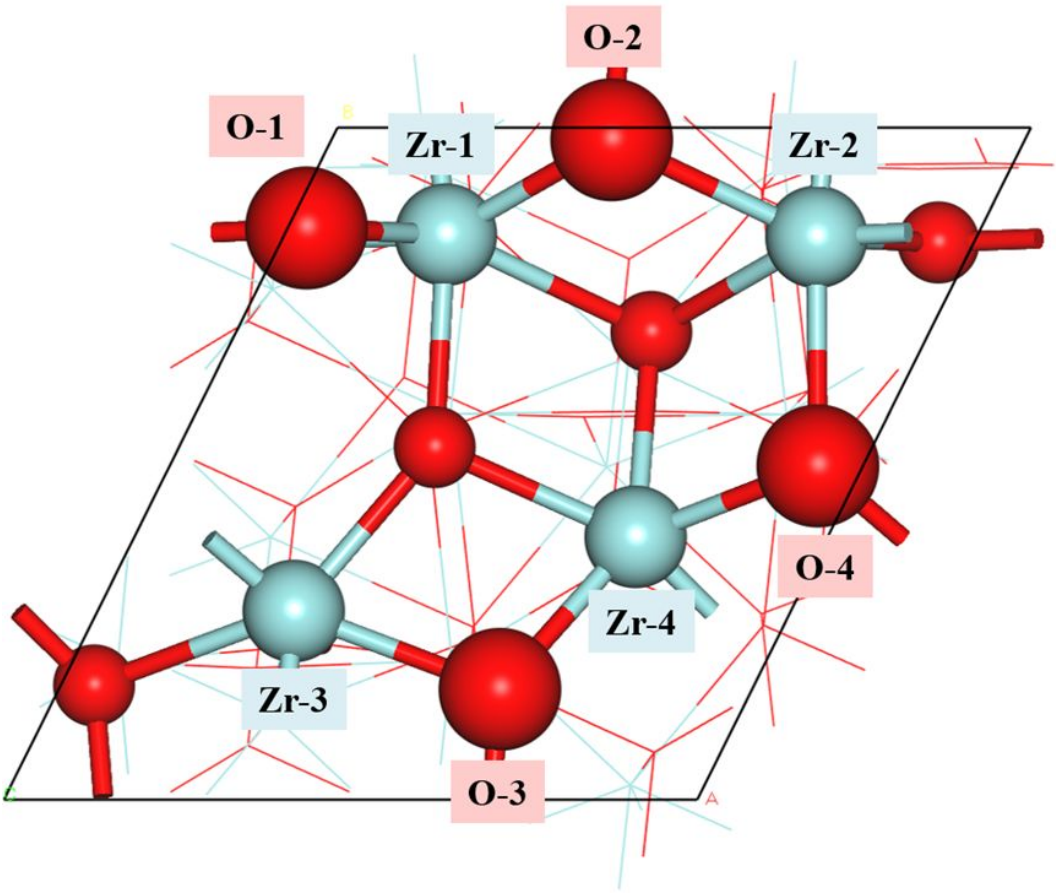

Figure S9. Different Zr or O sites on m-ZrO_2 (-111) surface.

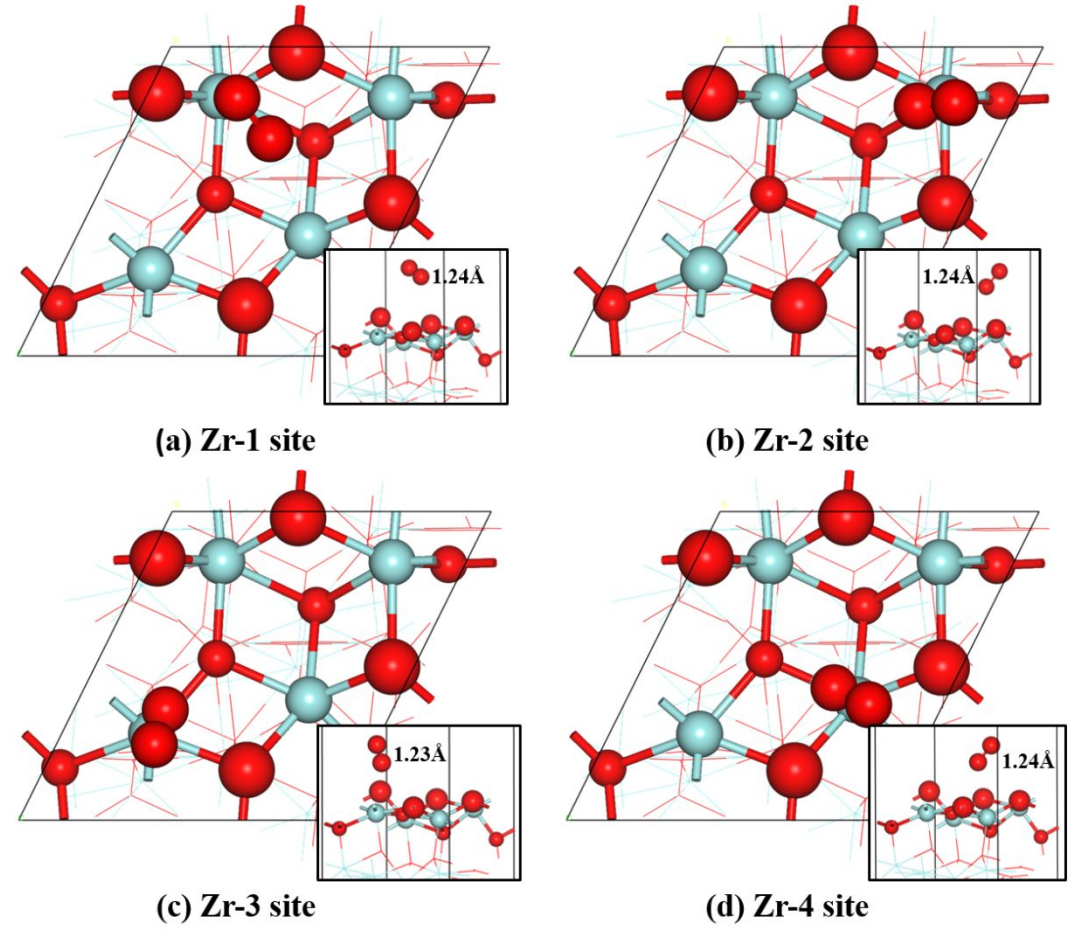

Figure S10. The optimized structures of O_2 adsorptions on (a) Zr-1 site, (b) Zr-2 site, (c) Zr-3 site and (d) Zr-4 site of m-ZrO_2 (-111) surface.

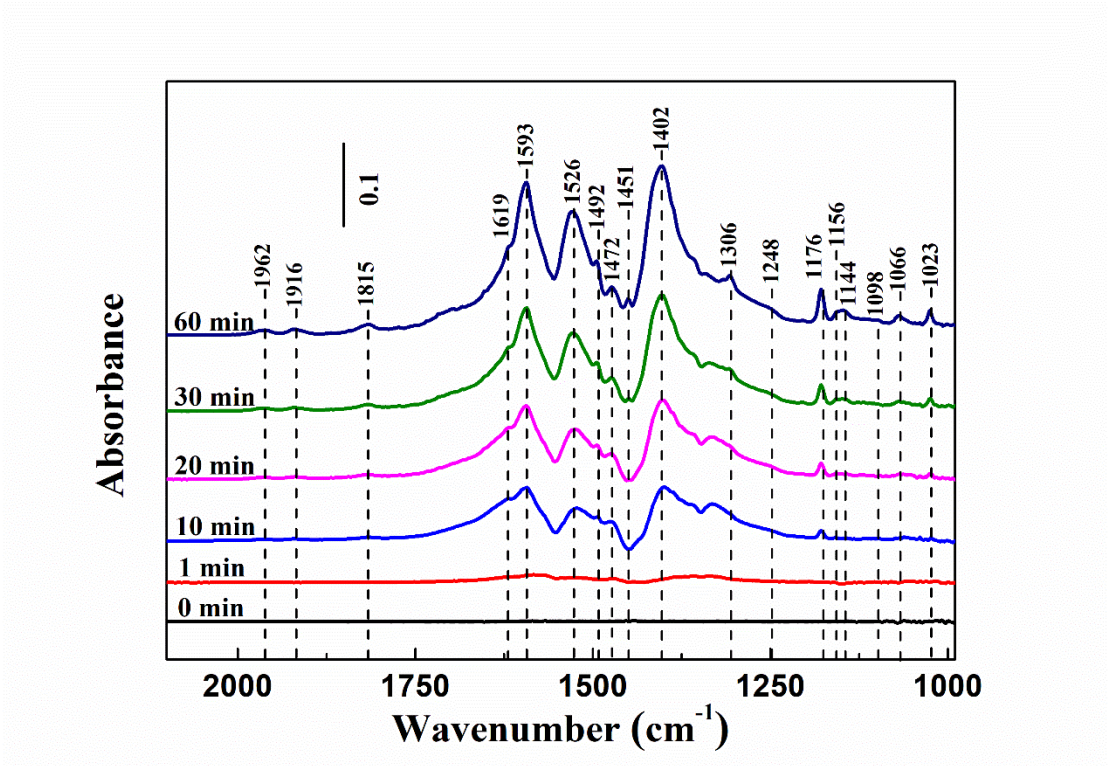

Figure S11. Dynamic changes of *in situ* DRIFTS of MB-0.3 sample as a function of time in a flow of O_2 + toluene + N_2 at 240 ºC. Reaction conditions: 1000 ppm toluene and 20% O_2 balanced by N_2. The total flow rate was 50 mL min^{-1}.

References

(1) Kresse, G.; Furthmüller, J. Efficient Iterative Schemes for ab initio Total-Energy Calculations Using a Plane-Wave Basis Set. *Physical Review B* **1996,** *54* (16), 11169-11186.

(2) Perdew, J. P.; Burke, K.; Ernzerhof, M. Generalized Gradient Approximation Made Simple. *Physical Review Letters* **1996,** *77* (18), 3865-3868.

(3) Blöchl, P. E. Projector Augmented-Wave Method. *Physical Review B* **1994,** *50* (24), 17953-17979.

(4) Kresse, G.; Joubert, D. From Ultrasoft Pseudopotentials to the Projector Augmented-Wave Method. *Physical Review B* **1999,** *59* (3), 1758-1775.

(5) Piskorz, W.; Gryboś, J.; Zasada, F.; Cristol, S.; Paul, J.-F.; Adamski, A.; Sojka, Z. Periodic Dft and Atomistic Thermodynamic Modeling of the Surface Hydration Equilibria and Morphology of Monoclinic ZrO_2 Nanocrystals. *J. Phys. Chem. C* **2011,** *115* (49), 24274-24286.

(6) Monkhorst, H. J.; Pack, J. D. Special Points for Brillouin-Zone Integrations. *Physical Review B* **1976,** *13* (12), 5188-5192.

(7) Grau-Crespo, R.; Hernández, N. C.; Sanz, J. F.; de Leeuw, N. H. Theoretical Investigation of the Deposition of Cu, Ag, and Au Atoms on the ZrO_2(111) Surface. *J. Phys. Chem. C* **2007,** *111* (28), 10448-10454.
(8) Cai, Q.; Lopez-Ruiz, J. A.; Cooper, A. R.; Wang, J.-g.; Albrecht, K. O.; Mei, D. Aqueous-Phase Acetic Acid Ketonization over Monoclinic Zirconia. *ACS Catal.* **2018,** *8* (1), 488-502.
(9) A., C. E.; A., R.; H., d. L. N. Density Functional Theory Study of Ni Clusters Supported on the ZrO_2(111) Surface. *Fuel Cells* **2017,** *17* (2), 125-131.
(10) Korhonen, S. T.; Calatayud, M.; Krause, A. O. I. Stability of Hydroxylated ($\bar{1}$11) and ($\bar{1}$01) Surfaces of Monoclinic Zirconia: A Combined Study by Dft and Infrared Spectroscopy. *J. Phys. Chem. C* **2008,** *112* (16), 6469-6476.
(11) Jing, M.; Song, W.; Chen, L.; Ma, S.; Deng, J.; Zheng, H.; Li, Y.; Liu, J.; Zhao, Z. Density Functional Theory Study of the Formaldehyde Catalytic Oxidation Mechanism on a Au-Doped CeO_2(111) Surface. *J. Phys. Chem. C* **2018,** *122* (1), 438-448.
(12) Oyama, S. T.; Zhang, X.; Lu, J.; Gu, Y.; Fujitani, T. Epoxidation of Propylene with H_2 and O_2 in the Explosive Regime in a Packed-Bed Catalytic Membrane Reactor. *J. Catal.* **2008,** *257* (1), 1-4.
(13) Liu, Y.; Dai, H.; Deng, J.; Du, Y.; Li, X.; Zhao, Z.; Wang, Y.; Gao, B.; Yang, H.; Guo, G. In Situ Poly(Methyl Methacrylate)-Templating Generation and Excellent Catalytic Performance of MnO_x/3DOM $LaMnO_3$ for the Combustion of Toluene and Methanol. *Appl. Catal., B* **2013,** *140–141*, 493-505.
(14) Zou, X.; Rui, Z.; Song, S.; Ji, H. Enhanced Methane Combustion Performance over $NiAl_2O_4$-Interface-Promoted Pd/γ-Al_2O_3. *J. Catal.* **2016,** *338*, 192-201.